LETTERS

Gamma-band synchronization in visual cortex predicts speed of change detection

Thilo Womelsdorf[1]*, Pascal Fries[1,2]*, Partha P. Mitra[3] & Robert Desimone[4,5]

Our capacity to process and respond behaviourally to multiple incoming stimuli is very limited. To optimize the use of this limited capacity, attentional mechanisms give priority to behaviourally relevant stimuli at the expense of irrelevant distractors. In visual areas, attended stimuli induce enhanced responses and an improved synchronization of rhythmic neuronal activity in the gamma frequency band (40–70 Hz)[1–11]. Both effects probably improve the neuronal signalling of attended stimuli within and among brain areas[1,12–16]. Attention also results in improved behavioural performance and shortened reaction times. However, it is not known how reaction times are related to either response strength or gamma-band synchronization in visual areas. Here we show that behavioural response times to a stimulus change can be predicted specifically by the degree of gamma-band synchronization among those neurons in monkey visual area V4 that are activated by the behaviourally relevant stimulus. When there are two visual stimuli and monkeys have to detect a change in one stimulus while ignoring the other, their reactions are fastest when the relevant stimulus induces strong gamma-band synchronization before and after the change in stimulus. This enhanced gamma-band synchronization is also followed by shorter neuronal response latencies on the fast trials. Conversely, the monkeys' reactions are slowest when gamma-band synchronization is high in response to the irrelevant distractor. Thus, enhanced neuronal gamma-band synchronization and shortened neuronal response latencies to an attended stimulus seem to have direct effects on visually triggered behaviour, reflecting an early neuronal correlate of efficient visuo-motor integration.

Two monkeys were trained to perform a change detection task while spikes and local field potentials (LFPs) were recorded from several electrodes in area V4 (Fig. 1a, b; see Methods for details), an area that is strongly modulated by attention[3–5]. Local synchronization was assessed by the coherence spectrum between spike trains and LFPs, as well as the power spectrum of the LFPs. We previously found that visual stimuli induced gamma-band synchronization in V4, which was enhanced when the stimulus was attended[4] (Fig. 1c). Here we use data from our previous study in a new analysis that focuses on the behavioural reaction times to the stimulus change and on any associated changes in power, coherence and firing rates, time resolved in successive 10-ms steps with a sliding analysis window of ±125 ms.

We first calculated LFP power ($n = 64$ recording sites) and spike–LFP coherence ($n = 244$ pairs of recordings sites) in the gamma frequency band (40–72 Hz), as well as firing rates ($n = 61$ recording sites) separately for the 25% trials with the slowest behavioural reactions and the 25% trials with the fastest reactions. Spike–field coherence from one pair of recording sites is shown in Fig. 2. Both in this example and across the set of recordings, we found that trials

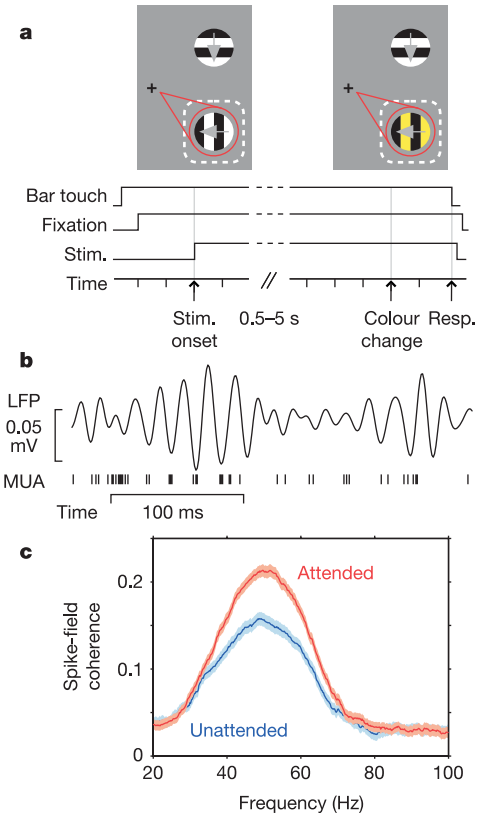

Figure 1 | Stimuli, behavioural model and examples of gamma-band synchronization and its modulation by attention. a, Monkeys started a trial by touching the bar and directing gaze to the fixation point. After a baseline period, two stimuli were presented, one inside the receptive field of the recorded neurons (broken rectangle) and one outside. On separate trials and before stimulus presentation, monkeys were cued to attend to one of the stimulus locations (red spotlight) and ignore the other. They were rewarded for releasing the bar on a subtle colour change in the cued stimulus while ignoring equally likely changes of the uncued stimulus. Changes could occur at any moment between 0.5 and 5 s after stimulus onset. **b**, Example of rhythmic multiunit activity (MUA) that is synchronized to gamma-band oscillations in the LFP. Multiunit activity and LFP were recorded from two separate electrodes. **c**, Example of spike–field coherence as a function of frequency for one pair of recording sites. The red (blue) lines show data recorded when the monkey directed attention into (away from) the receptive field of the recorded neurons. Shaded regions indicate ±1 s.e.m.

[1]FC Donders Centre for Cognitive Neuroimaging, Radboud University Nijmegen, 6525 EN Nijmegen, The Netherlands. [2]Department of Biophysics, Radboud University Nijmegen, 6525 EZ Nijmegen, The Netherlands. [3]Cold Spring Harbor Laboratory, Cold Spring Harbor, New York 11724, USA. [4]Laboratory of Neuropsychology, National Institute of Mental Health, National Institutes of Health, Bethesda, Maryland 20892, USA. [5]McGovern Institute for Brain Research at MIT, Cambridge, Massachusetts 02139, USA.
*These authors contributed equally to this work.

leading to fast reaction times contained more gamma-band power (Fig. 3a) and gamma-band spike–field coherence (Fig. 3b) during epochs before and after the stimulus change event. The earliest significant change was found for spike–field coherence at 350 ms preceding the change event, whereas gamma-band power in the LFP was significantly enhanced ~125 ms before the stimulus change. Because of the ±125-ms width of the analysis window, we cannot precisely localize the beginning of these effects in time, although it is clear that they begin before the change event itself. Thus, enhanced gamma-band synchrony seems to lead to faster behavioural responses. Spike rates analysed with the same ±125-ms analysis window that was used for the spectral analysis showed a significant increase beginning 50 ms before the change event in trials leading to fast reaction times (Fig. 3c). Given the width of the analysis window, this could be an enhanced visual response to the change event itself.

In addition to these neuronal effects before the change event, all measures showed stronger gamma-band synchrony and spike rates in response to the change event on fast trials. On average, fast reactions were associated with a relative gamma-band power enhancement of 14.1% in the analysis windows centred between 0 and 75 ms after the change event, and an average spike rate enhancement of 8%. We did not consider effects beyond 75 ms after the change event, because the ±125-ms analysis window in this case would include the time of the earliest behavioural responses, which could be as fast as 200 ms (see Supplementary Fig. 1). We also computed spike rates on the basis of a narrower analysis window (gaussian with s.d. of 10 ms) and found that trials with fast reactions had shorter response onset latencies to the change event (~10–20 ms), and an enhanced evoked response to the stimulus in the period from 40 to 130 ms after the stimulus change (Fig. 3d).

The response and coherence differences found on fast versus slow trials could be selective to the attended stimulus, or they could be due to a general increase in arousal, or alertness, on trials with fast reaction times[17]. If the latter is true, we would expect enhanced gamma-band power and coherence also on trials with rapid behavioural responses to the stimulus outside the receptive field of the recorded neurons. We therefore computed power, coherence and firing rates in response to the stimulus inside the receptive field when the monkey was attending to a stimulus outside the receptive field and around the time of the change of this attended stimulus outside the receptive field. In contrast to the results when the monkey responded to the stimulus change inside the receptive field, gamma-band power and coherence at the unattended location were significantly reduced throughout most of the pre-change period when the monkeys responded quickly to the stimulus outside the receptive field (Fig. 3e, f). Spike rates were only marginally reduced for fast versus slow trials (Fig. 3g). Thus, the effects of attention on LFP power and coherence inside the receptive field were approximately reversed for fast versus slow responses to attended stimuli outside the receptive field (Fig. 3h), which is inconsistent with a general change in arousal.

These results suggest that when the monkey attends to one stimulus and ignores a distractor, the relative gamma-band coherence differences in response to the attended and ignored stimulus will, on average, predict fast versus slow reaction times well before the change event occurs. When the change event occurs, neuronal responses have a shorter latency and stronger gamma-band coherence on the faster trials. Some of the observed effects became apparent already in the first analysis window, 500 ms before the change event—that is, the time of stimulus onset for the shortest

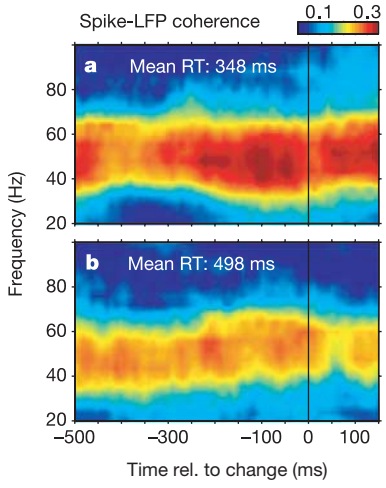

Figure 2 | Spike–field coherence from one pair of recording sites. Shown are averages over the 25% of trials with the fastest (**a**) and the slowest (**b**) reaction times.

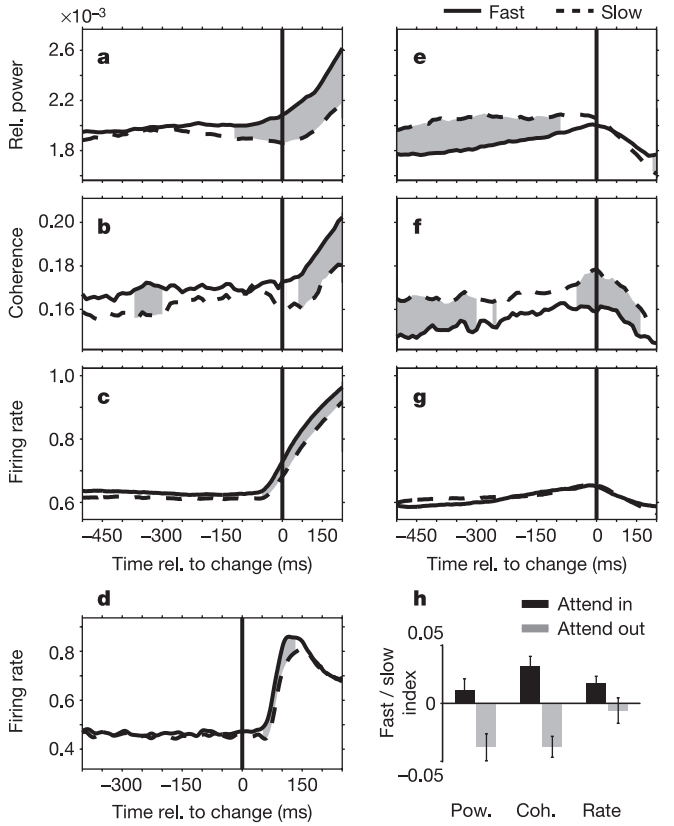

Figure 3 | Neuronal activity parameters in trials with fast and slow change detection. **a**–**d**, Time course of neuronal activity parameters induced by the attended stimulus inside the receptive fields around the change of the attended stimulus. **a**, Relative LFP power in the gamma band (40–72 Hz). **b**, Spike–field coherence in the gamma band. **c**, **d**, Firing rate. In **a**–**c**, analysis windows of ±125 ms were used; in **d**, a gaussian kernel of 10-ms s.d. was used. Shown are grand averages calculated separately for the 25% of trials with the fastest (unbroken lines) and slowest (broken lines) behavioural responses. Grey shading indicates significance (two-sided paired *t*-test, $P < 0.05$ after multiple comparison correction). **e**–**g**, As **a**–**c**, but showing the time course of neuronal activity parameters induced by the ignored distractor, around the change of the attended stimulus that was outside the receptive fields. **h**, Comparison of neuronal activity parameters for fast versus slow trials (average over −500 to −125 ms preceding the change) when behavioural reports were in response to changes inside (black bars) or outside (grey bars) the receptive fields. Shown is the modulation index defined as $(P_{fast} - P_{slow})/(P_{fast} + P_{slow})$, where P_{fast} is one of the parameters investigated for trials with fast responses and P_{slow} is one for trials with slow responses. Error bars denote ±1 s.e.m. Pow., power; Coh., coherence.

trials. To determine the earliest neural effects on reaction time, we therefore repeated the above analyses for a 250-ms window before stimulus onset, but we found no significant effects in that interval.

To test directly whether trial-by-trial fluctuations of synchrony could predict the speed of change detection on a single-trial basis, we performed a correlation analysis. For this, we correlated trial-by-trial variations in reaction time with trial-by-trial variations in coherence or power and firing rate (see Methods). To obtain an overview of the spectral specificity of the neuronal response changes, we extended the time-resolved analysis to frequencies of 8–100 Hz. Consistent with the preceding analysis, we found that short reaction times were predicted by enhanced power and coherence in the gamma-frequency band (40–72 Hz) in time epochs preceding the stimulus change by several hundred milliseconds (Fig. 4a, b). Also shortly before and after the change event, behavioural response times were predicted by the degree of synchrony and neuronal response magnitude. Correlations of firing rate (analysed within the same sliding ±125-ms analysis window used above) and reaction time were significant from 40 ms before the change and onwards (Fig. 4c). In contrast to firing rate and gamma-band modulation, we observed reduced power in the alpha (10 Hz) and beta (15 Hz) frequency bands for fast trials in a restricted time window starting 80 ms before the stimulus change (Fig. 4a).

Across measures, the strongest correlations with reaction times were evident at a time immediately after the stimulus change. To analyse this effect for single recording sites, we calculated *Z*-scores of the correlation of reaction time with gamma-band power and spike rate averaged over the analysis windows centred between 0 and 75 ms after the change event. The distribution of *Z*-scores for LFP power and firing rate is strongly biased towards negative values (see Supplementary Fig. 2 and Supplementary Table). Moreover, the negative reaction time correlations are clearly evident in both monkeys, which is noteworthy because the two monkeys showed a different trend in reaction time speed as a function of time in trial (namely, a slightly increasing/decreasing response speed with time in trial; see Supplementary Fig. 1 and Supplementary Note). Thus, while the two monkeys showed weak but opposite trends in reaction times across the trial, they both showed the same patterns of correlation between reaction times and spectral power, firing rate and coherence.

Our results show that the degree of neuronal synchrony in the gamma-frequency band in time intervals preceding and following a behaviourally relevant sensory change can predict the speed of behavioural responses to that change. These effects are reversed for responses to stimulus changes outside the receptive field.

The neuronal processes in visual area V4, studied here, constitute only one link in the processing chain from the stimulus change event to its behavioural report. Oscillatory synchronization within and between other structures along this way has been described and probably also has a functional role[16,18–24]. Enhanced gamma-band synchronization in V4 could be directly involved in the detection process and/or in the signalling of the detection achieved in V4 or a preceding area. In both cases, enhanced gamma-band synchronization among the recorded neurons probably subserves rapid and reliable signalling mechanistically, because it results in efficient summation of postsynaptic potentials[13,25,26].

A reported effect of gamma-band synchronization during the onset of visual stimuli is enhanced synchronization and shortened response latencies of the first spikes on stimulus presentation[27]. If this finding is extended to stimulus changes, in addition to stimulus onsets, it suggests that there is a mechanistic link between enhanced gamma-band synchrony around the time of the sensory change and the more rapid, shifted response latency that we observe. Taken together, our results suggest that the enhanced precise synchronization is instrumental in subserving a rapid and reliable transmission of information about sensory changes to the postsynaptic targets and thus ultimately triggers enhanced detection efficiency.

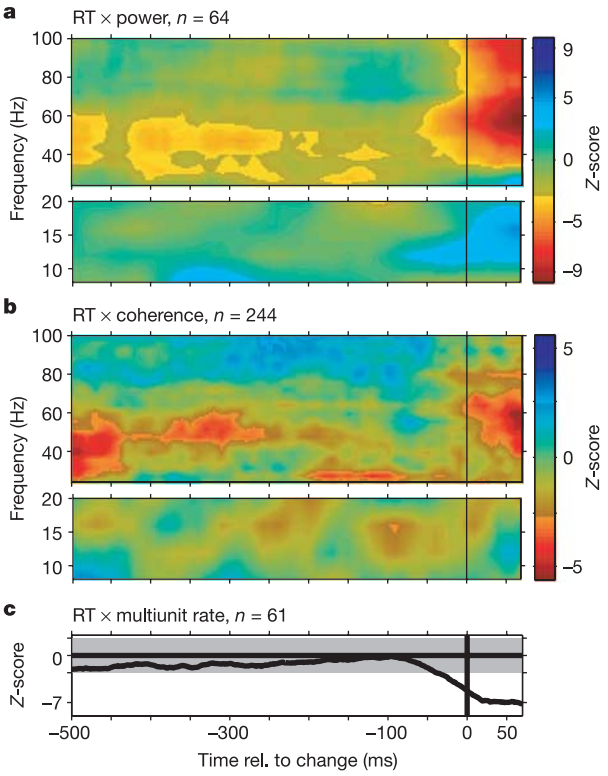

Figure 4 | Trial-by-trial prediction of reaction times by neuronal activity. Shown are *Z*-scores of correlation coefficients pooled across monkeys and recordings sites (**a**, **c**) or pairs of recording sites (**b**) on the basis of analysis windows of ±125 ms. Note inverted colour scale. Grey shading highlights significance (99% confidence). Results are shown separately for lower and higher frequencies because different spectral concentrations were used (see Methods). **a**, LFP power versus reaction times. **b**, Spike–field coherence versus reaction times. **c**, Firing rates versus reaction times.

METHODS

Procedures were done in accordance with NIH guidelines and were approved by the National Institute of Mental Health (NIMH) Intramural Animal Care and Use Committee. Simultaneous recordings of spikes and local field potentials were made from four to eight electrodes in visual areas V4 in two hemispheres of two monkeys. In total, multiunit recordings were obtained from 61 sites (39 and 22 in monkey A and B, respectively) and LFP recordings from 64 sites (40 and 24, respectively). Power and coherence spectra were assessed for windows of ±125 ms, moved over the data in steps of 10 ms from 500 ms before to 150 ms after the stimulus change. Neuronal activity parameters were compared between trials with the 25% fastest and trials with the 25% slowest response times of individual recording sessions. The mean reaction time for the fast and slow trials was 346 ms and 490 ms, respectively (median, 359 and 485 ms, respectively). To determine the predictive capability of neuronal activity parameters for reaction time, we calculated the Pearson correlation coefficient between the trial-by-trial variations in reaction times and the trial-by-trial variations in power, coherence and spike rate. See Supplementary Methods for more information.

Received 1 June; accepted 23 September 2005.
Published online 21 December 2005.

1. Engel, A. K., Fries, P. & Singer, W. Dynamic predictions: oscillations and synchrony in top-down processing. *Nature Rev. Neurosci.* **2,** 704–716 (2001).
2. Desimone, R. & Duncan, J. Neural mechanisms of selective visual attention. *Annu. Rev. Neurosci.* **18,** 193–222 (1995).
3. Motter, B. C. Neural correlates of attentive selection for colour or luminance in extrastriate area V4. *J. Neurosci.* **14,** 2178–2189 (1994).
4. Fries, P., Reynolds, J. H., Rorie, A. E. & Desimone, R. Modulation of oscillatory neuronal synchronization by selective visual attention. *Science* **291,** 1560–1563 (2001).

5. Bichot, N. P., Rossi, A. F. & Desimone, R. Parallel and serial neural mechanisms for visual search in macaque area V4. *Science* **308,** 529–534 (2005).
6. Treue, S. & Maunsell, J. H. Attentional modulation of visual motion processing in cortical areas MT and MST. *Nature* **382,** 539–541 (1996).
7. Cook, E. P. & Maunsell, J. H. Dynamics of neuronal responses in macaque MT and VIP during motion detection. *Nature Neurosci.* **5,** 985–994 (2002).
8. Steinmetz, P. N. *et al.* Attention modulates synchronized neuronal firing in primate somatosensory cortex. *Nature* **404,** 187–190 (2000).
9. Taylor, K., Mandon, S., Freiwald, W. A. & Kreiter, A. K. Coherent oscillatory activity in monkey area V4 predicts successful allocation of attention. *Cereb. Cortex* **15,** 1424–1437 (2005).
10. Gruber, T., Müller, M. M., Keil, A. & Elbert, T. Selective visual–spatial attention alters induced gamma band responses in the human EEG. *Clin. Neurophysiol.* **110,** 2074–2085 (1999).
11. Martinez, A. *et al.* Involvement of striate and extrastriate visual cortical areas in spatial attention. *Nature Neurosci.* **2,** 364–369 (1999).
12. Salinas, E. & Sejnowski, T. J. Impact of correlated synaptic input on output firing rate and variability in simple neuronal models. *J. Neurosci.* **20,** 6193–6209 (2000).
13. Salinas, E. & Sejnowski, T. J. Correlated neuronal activity and the flow of neural information. *Nature Rev. Neurosci.* **2,** 539–550 (2001).
14. Tiesinga, P. H. & Sejnowski, T. J. Rapid temporal modulation of synchrony by competition in cortical interneuron networks. *Neural Comput.* **16,** 251–275 (2004).
15. Börgers, C., Epstein, S. & Kopell, N. J. Background gamma rhythmicity and attention in cortical local circuits: A computational study. *Proc. Natl Acad. Sci. USA* **102,** 7002–7007 (2005).
16. Schoffelen, J. M., Oostenveld, R. & Fries, P. Neuronal coherence as a mechanism of effective corticospinal interaction. *Science* **308,** 111–113 (2005).
17. Munk, M. H., Roelfsema, P. R., König, P., Engel, A. K. & Singer, W. Role of reticular activation in the modulation of intracortical synchronization. *Science* **272,** 271–274 (1996).
18. Lee, D. Coherent oscillations in neuronal activity of the supplementary motor area during a visuomotor task. *J. Neurosci.* **23,** 6798–6809 (2003).
19. Riehle, A., Grün, S., Diesmann, M. & Aertsen, A. Spike synchronization and rate modulation differentially involved in motor cortical function. *Science* **278,** 1950–1953 (1997).
20. Mehring, C. *et al.* Inference of hand movements from local field potentials in monkey motor cortex. *Nature Neurosci.* **6,** 1253–1254 (2003).
21. Pesaran, B., Pezaris, J. S., Sahani, M., Mitra, P. P. & Andersen, R. A. Temporal structure in neuronal activity during working memory in macaque parietal cortex. *Nature Neurosci.* **5,** 805–811 (2002).
22. Scherberger, H., Jarvis, M. R. & Andersen, R. A. Cortical local field potential encodes movement intentions in the posterior parietal cortex. *Neuron* **46,** 347–354 (2005).
23. Gonzalez Andino, S. L., Michel, C. M., Thut, G., Landis, T. & Grave de Peralta, R. Prediction of response speed by anticipatory high-frequency (gamma band) oscillations in the human brain. *Hum. Brain Mapp.* **24,** 50–58 (2005).
24. Gray, C. M., König, P., Engel, A. K. & Singer, W. Oscillatory responses in cat visual cortex exhibit inter-columnar synchronization which reflects global stimulus properties. *Nature* **338,** 334–337 (1989).
25. Azouz, R. & Gray, C. M. Adaptive coincidence detection and dynamic gain control in visual cortical neurons in vivo. *Neuron* **37,** 513–523 (2003).
26. MacLeod, K., Bäcker, A. & Laurent, G. Who reads temporal information contained across synchronized and oscillatory spike trains? *Nature* **395,** 693–698 (1998).
27. Fries, P., Neuenschwander, S., Engel, A. K., Goebel, R. & Singer, W. Rapid feature selective neuronal synchronization through correlated latency shifting. *Nature Neurosci.* **4,** 194–200 (2001).

Supplementary Information is linked to the online version of the paper at www.nature.com/nature.

Acknowledgements We thank J. H. Reynolds, A. E. Rorie and A. F. Rossi for help with experiments; and R. Oostenveld and M. Bauer for discussions. This research was supported by grants from the Human Frontier Science Program Organization (to P.F. and P.P.M.), The Netherlands Organization for Scientific Research and The Volkswagen Foundation (to P.F.), the NIH (to P.P.M.) and the Intramural Program of the NIH, NIMH.

Author Contributions T.W. and P.F. contributed equally to this work. P.F. conceived and performed the experiment. T.W., P.F. and P.P.M. conceived and performed the data analysis. P.F., T.W. and R.D. wrote the paper.

Author Information Reprints and permissions information is available at npg.nature.com/reprintsandpermissions. The authors declare no competing financial interests. Correspondence and requests for materials should be addressed to T.W. (t.womelsdorf@fcdonders.ru.nl).

Supplementary Methods:

Gamma-band synchronization in visual cortex predicts speed of change detection

Thilo Womelsdorf[*], Pascal Fries[*], Partha P. Mitra, Robert Desimone

[*]These authors contributed equally to this work.

Neurophysiological recording techniques and LFP preprocessing:

Neuronal recordings were made from two hemispheres in two monkeys through chambers implanted over area V4 during surgeries conducted under aseptic conditions with isofluorane anesthesia. Before recording, four to eight tungsten microelectrodes (impedances of 1-2 MΩ) were advanced separately at a very slow rate (1.5 mm/s) to minimize deformation of the cortical surface by the electrode ("dimpling"). Electrodes tips were separated by 650 or 900 μm. Data amplification, filtering and acquisition were done with a Multichannel Acquisition Processor from Plexon Incorporated. The signal from each electrode was passed through a headstage with unit gain and an output impedance of 240 Ω and then split to separately extract the spike and the LFP components. For spike recordings, the signals were filtered with a passband of 100-8000 Hz, further amplified and digitized with 40 kHz. A threshold was set interactively and spike waveforms were stored for a time window from 150 μs before to 700 μs after threshold crossing. The threshold clearly separated spikes from noise, but was chosen to include multi-unit activity. Offline, we performed a principal component analysis of the waveforms and plotted the first against the second principal component. Those waveforms that corresponded to artifacts were excluded. For multi-unit analyses, all other waveforms were accepted and the times of threshold crossing were kept and down-sampled to 1 kHz. For LFP recordings, the signals were filtered with a passband of 0.7-170 Hz, further amplified and digitized at 1 kHz. The powerline artifact was removed from the LFP using the following procedure: All signals had been recorded continuously for the entire duration of the recording session. For each time epoch of interest (and each recording channel), we first took a 10 second epoch out of the continuous signal with the epoch of interest in the middle. We then calculated the Discrete Fourier Transform (DFT) of the 10 s epoch at 50 Hz, 100 Hz and 150 Hz without any tapering. Since the powerline artifact is of a perfectly constant frequency, the 10 s epoch contains integer cycles of the artifact frequencies

and all the artifact energy is contained in those DFTs. We then constructed 50 Hz-, 100 Hz- and 150 Hz-sine waves with the amplitudes and phases as estimated by the respective DFTs and subtracted those sine waves from the 10 s epoch. The epoch of interest was then cut out of the cleaned 10 s epoch. Power spectra of the cleaned 10 s epochs demonstrated that all artifact energy was eliminated, leaving a notch of a bin width of 0.1 Hz (=1/10 s). The actual spectral analysis used the multi-taper method, with a spectral smoothing of ± 4 Hz (for frequencies between 8 and 20 Hz) or ± 16 Hz (for frequencies between 20 and 100 Hz). Thus, the notch typically became invisible.

Time-frequency spectral analysis based on multitapering:

For the assessment of power and coherence spectra, we used windows of ± 125 ms length that were moved over the data in steps of 10 ms from 500 ms before to 150 ms after the stimulus change. For each window, we applied mutitaper methods to achieve optimal spectral concentration[1-3]. Multitapering involves the multiplication of data segments with multiple tapers before Fourier transformation. Tapering effectively concentrates spectral estimates across a specified frequency band. We used two different sets of tapers: For the low frequency range (8 to 20 Hz), we chose a spectral concentration over ± 4 Hz, while for the high frequency range (20 to 100 Hz), we chose a spectral concentration over ± 16 Hz.

For each taper, the data epoch was multiplied with that taper and then Fourier transformed, giving the windowed Fourier transform, $\tilde{x}_k(f)$:

$$\tilde{x}_k(f) = \sum_{1}^{N} w_k(t) x_t e^{-2\pi i f t}$$

where x_t, $(t = 1,2,...,N)$ is the time series of the signal under consideration and $w_k(t)$, $(k = 1,2,...,K)$ are K orthogonal taper functions.

The multitaper estimates for the spectrum $S_x(f)$ and the cross-spectrum $S_{yx}(f)$ are given by

$$S_x(f) = \frac{1}{K} \sum_{1}^{K} \left| \tilde{x}_k(f) \right|^2$$

$$S_{yx}(f) = \frac{1}{K} \sum_{1}^{K} \tilde{y}_k(f) \tilde{x}_k^*(f)$$

Spectra and cross-spectra are averaged over trials before calculating the coherency

$$C_{yx}(f) = \frac{S_{yx}(f)}{\sqrt{S_x(f)S_y(f)}}$$

Coherency is a complex quantity. Its absolute value is termed coherence and ranges from 0 to 1. A coherence value of 1 indicates that the two signals have a constant phase relationship (and amplitude covariation), a value of 0 indicates the absence of any phase relationship.

Coherence estimates have a positive bias that decreases with an increase in the amount of data. To correct for this, a non-linear transformation was applied to the coherence spectra[1], which will be referred to as a z-transformation. If C is the untransformed coherence estimate and ν is the degrees of freedom (two times the total number of tapers applied), then the variable

$$q = \sqrt{-(\nu - 2)\log(1 - |C|^2)}$$

has a Raleigh distribution with density

$$p(q) = qe^{-q^2/2}.$$

This density function does not depend on ν and furthermore has a tail that closely resembles a Gaussian. For certain values of a fitting parameter β, a further linear transformation

$$r = \beta(q - \beta)$$

leads to a distribution that closely resembles a standard normal Gaussian for r > 2. We therefore refer to r as the z-transformed coherence. A reasonable choice for β is 23/20.

Spike-field coherence was calculated with spikes and LFP from the same and from different electrodes. Restricting the SFC analysis to SFCs with spikes and LFP from different electrodes left the results unchanged.

Neural activity sorted according to reaction time:

We assessed power, coherence and spike rate for trials with the 25 % fastest and 25 % slowest reaction times of individual recording sessions. The mean RT for the subset of fast (slow) trials was 346 ms (490 ms) (median: 359 ms / 485 ms). This separation

ensured the least overlap of fast and slow reaction time bins across recording sites (such that slowest reaction times in the fast bin did not overlap with the fastest reaction times in the slow bin across sessions), while providing as much neural data as possible to calculate the spectral estimates. Moreover, percentile separation ensures an equal number of trials in each subset and thereby eliminates sampling biases[1].

We wanted to test whether the variable *gamma-band power* (or *gamma-band spike field coherence*, or *firing rate*) differed between the conditions *fast response* and *slow response*. Therefore, we calculated t-values for the difference between the two conditions and across recording sites (or pairs of sites), separately for all time windows in the sliding window analysis. We performed a correction for the multiple comparisons done, using a non-parametric permutation approach for significance testing[4,5]. To this end, the following procedure was performed 10000 times: For each recordings site (or pair of sites), a random decision was made to either exchange the two conditions (50% probability) or leave them unchanged (50% probability). Subsequently, paired t-tests were determined across the sites (or pairs of sites) between the two conditions and for all time windows. The maximal and the minimal t-value across all time windows was kept, resulting in 10000 maximal and 10000 minimal t-values. From this empirical distribution of global maxima and minima, we determined the 2.5 % and the 97.5 % points, t(global,2.5 %) and t(global,97.5 %). For each time window, we then determined the t-value between the non-randomized conditions. The non-randomized t-value for a given time window was considered significant if it was larger than t(global,97.5 %) or less than t(global,2.5 %). This procedure corresponds to a two-sided test with a global false positive rate of 5 % and corrects for the multiple comparisons across the time interval.

Correlation analysis:

To determine the predictive capability of neuronal activity parameters for reaction time, we calculated the Pearson correlation coefficient between the trial-by-trial variations in reaction times and the trial-by-trial variations of power, coherence and spike rate. This was done separately for each analyzed time window and, in the case of power and coherence, separately for each analyzed frequency. Correlation coefficients were Fisher Z-transformed and those Fisher Z-values were transformed to z-scores. Z-scores were pooled across recording sites or pairs of sites according to:

$$z = \frac{1}{N}\sum_{i=1}^{N} z_i$$

with z_i being the z-score of the i-th recording site or pair of sites. Note that spike field coherence cannot be estimated directly for short time epochs of single trials. We therefore derived a new analysis method to obtain single-trial coherence estimates based on z-transformed coherence values as outlined in the following paragraph.

Estimation of spike-field coherence of single-trials:

Coherence cannot be estimated directly for single short data epochs (of two signals). The reason is that coherence is in itself a statistic about the distribution of phase differences between the two signals, that requires multiple estimates of this phase difference. Here, we aimed at estimating the correlation between variations of reaction times across trials and variations of spike-field coherence across trials. We furthermore aimed at doing this for short (250 ms) time windows, that cannot be reasonably cut into a sufficient number of pieces, nor allow the application of a sufficient number of multi-tapers to estimate coherence directly from the single trial data. In order to nevertheless obtain an estimate of single-trial coherence, we computed single-trial coherence pseudovalues (STCP). The rationale of this is that while we cannot determine the single-trial coherence directly, we can determine the coherence for all trials and we can also determine the coherence for all-but-one trials. For a linear function F of a sample S, the value of $F(S_i)$, i.e. the value of the function for the i-th observation, is identical to the pseudovalue

$$P = N \times F(S) - (N-1) \times F(S_{(i)}),$$

With $S_{(i)}$ being the entire sample with the i-th observation left out. We accordingly determined the $STCP$ for trial i as

$$STCP = N \times C(S) - (N-1) \times C(S_{(i)}),$$

with C being the z-transformed coherence.

Reference List

1. Jarvis, M.R. & Mitra, P.P. *Neural Comput.* **13**, 717-749 (2001).

2. Mitra, P.P. & Pesaran, B. *Biophys. J.* **76**, 691-708 (1999).

3. Pesaran, B., Pezaris, J.S., Sahani, M., Mitra, P.P. & Andersen, R.A. *Nat. Neurosci.* **5**, 805-811 (2002).

4. Maris, E. *Psychophysiology* **41**, 142-151 (2004).

5. Nichols, T.E. & Holmes, A.P. *Hum. Brain Mapp.* **15**, 1-25 (2001).

Supplementary Note:

Gamma-band synchronization in visual cortex predicts speed of change detection

Thilo Womelsdorf[*], Pascal Fries[*], Partha P. Mitra, Robert Desimone

[*]These authors contributed equally to this work.

The correlation between reaction times and neuronal activity is consistent across the two monkeys and it is not explained by a general effect of time-in-trial.

In principle, there might be a general effect of time-in-trial on both behavioral reaction times and neuronal activity that results in a correlation between those variables. This would not affect our conclusions. The finding that enhanced gamma-band synchronization results in rapid reaction times is physiologically most plausibly interpreted as a mechanistic link, irrespective of the source of the trial-by-trial variability in gamma-band synchronization. Furthermore, our data suggest that the correlation between reaction times and neuronal activity is actually not explained by a general effect of time-in-trial. A general effect of time-in-trial should affect reaction times and neuronal activity similarly and in both monkeys. However, we found that reaction times showed weak but opposite trends in the two monkeys. While reaction times decreased slightly with time-in-trial in one monkey, they increased slightly in the second monkey (Supplementary Figure 1**)**. We then analyzed the z-scores for the correlations between reaction times and gamma-band (40 - 72 Hz) power, gamma-band spike-field coherence and firing rate for the time period between the change event and 75 ms thereafter (Supplementary Figure 2). The Supplementary Table provides an overview of average correlations for all measures and both monkeys separately for the gamma-frequency band (40-72 Hz) and for the alpha/beta-frequency band (8-16 Hz). In both monkeys, the distribution of z-scores for the gamma-band is strongly biased towards negative values, both for gamma band power and spike-field coherence. Thus, while the two monkeys showed weak but opposite trends regarding the dependence of reaction times on time-in-trial, they both showed similar patterns of correlation between reaction times and spectral power and coherence.

Supplementary Table:

Gamma-band synchronization in visual cortex predicts speed of change detection

Thilo Womelsdorf[*], Pascal Fries[*], Partha P. Mitra, Robert Desimone

[*]These authors contributed equally to this work.

	LFP - power		Spike-field coherence	
	monkey P	monkey R	monkey P	monkey R
42-72 Hz	-0.05*** (68 %)	-0.10*** (100 %)	-0.01* (59 %)	-0.02* (58 %)
8-12 Hz	0.03** (70 %)	0.02 (58 %)	0 (44 %)	0.02*** (63 %)

Supplementary Table: Average Fisher z-transformed correlation coefficients for LFP-power and spike-field coherence with reaction time for monkey P and monkey R for the gamma frequency band and the alpha/beta frequency band. The correlations are averages of the analysis windows zero-centered within the time interval from 0 - 75 ms after the change event. Stars denote significance levels of correlations (* = $p<0.05$, ** = $p<0.01$, *** = $p<0.001$). The number in brackets show the proportion of cells with negative reaction time correlations (for the 42-72 Hz frequency range) and positive reaction time correlations (for the 8-12 Hz frequency range).

Supplementary Figure 1:

Gamma-band synchronization in visual cortex predicts speed of change detection

Thilo Womelsdorf[*], Pascal Fries[*], Partha P. Mitra, Robert Desimone

[*]These authors contributed equally to this work.

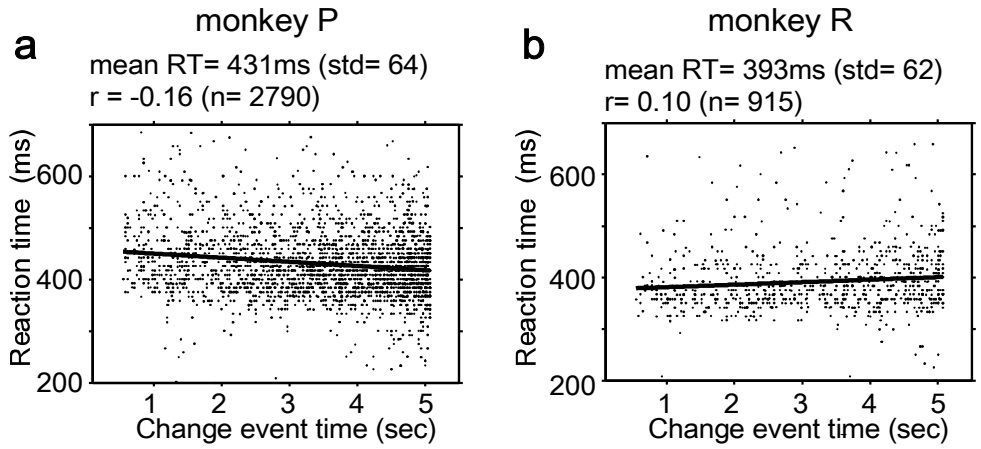

Supplementary Figure 1 Scatter plot of reaction times as a function of time after stimulus onset. The two panels show data from the two monkeys and each dot corresponds to the reaction time in a single trial.

Supplementary Figure 2:

Gamma-band synchronization in visual cortex predicts speed of change detection

Thilo Womelsdorf[*], Pascal Fries[*], Partha P. Mitra, Robert Desimone

[*]These authors contributed equally to the work.

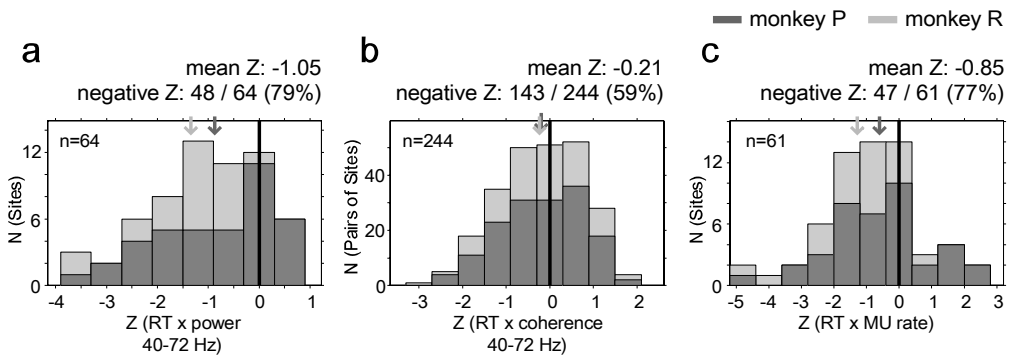

Supplementary Figure 2 Histograms of z-scores for the correlations between reaction times and gamma-band (40 - 72 Hz) power (**a**), gamma-band spike-field coherence (**b**) and firing rate (**c**). Histograms were compiled across individual recording sites (power and firing rate) or pairs of recording sites (coherence). Data from the two monkey are shown in black and grey, respectively. The z-scores were averaged across analysis windows centered on 0 - 75 ms after the change event. Black and grey arrows denote the average z-score of the distribution of the respective monkey.